Failure of Bolted Connections in an Aluminum Alloy

C.C. Menzemer, L. Fei, and T.S. Srivatsan

(Submitted 15 October 1998; in revised form 29 October 1998)

In structures built from either pure aluminum or aluminum-base alloys, plates are often used as connecting elements. Design of connections necessitates that consideration be given to all aspects related to mechanical failure of the fastener, distress of material adjacent to the fastener(s), and net-section tensile failure, including tear out of the fasteners. The shear failure of aluminum alloy connecting elements is the focus of this paper. Aluminum alloy 6061 was chosen, and an experimental study was performed with the objective of rationalizing block shear failure in connecting elements. Gusset plates were chosen, and samples representing four different bolt patterns were mechanically deformed. Models to estimate the capacity of the joints are examined and compared with experimental results. Mechanisms governing damage and failure are highlighted in light of the competing influences of load/stress distribution and intrinsic microstructural effects.

Keywords aluminum, bolted joints, failure model, gusset plates

1. Introduction

In a wide spectrum of structures made from either pure aluminum or aluminum-base alloys, plates of varying cross section have frequently been used as connecting links. Examples of such applications include (a) bracing systems and structural elements in rail-cars, (b) framing members in bulk transport vehicles and containers, (c) mounts for dump bodies, and (d) framing nodes for roof trusses. For practical situations demanding ease of application, familiarity with fabrication processes, and including the influence of severe dynamic loading, mechanical fasteners are preferred and often used. A successful design necessitates the need for an adequate consideration being provided in the event of failure of the mechanical fasteners, connection plate(s), and attaching members. Traditional mechanical and civil (structural) engineering design specifications have either opted to rely on models developed for structural steels or have been at the discretion of the design/practicing engineer (Ref 1, 2).

Mechanical fasteners have proven to successfully transfer load over relatively small areas. Consequently, critical design issues are normally associated with the transfer of concentrated forces (Ref 3). Failure of either a single rivet or bolt in a simple lap joint can occur as a result of either the independent or conjoint and mutually interactive influences of (a) shear failure of the fastener, (b) progressive bearing distress of adjacent material, (c) splitting of the sheet or plate near the hole in the direction of the applied load, and (d) tensile overload failure of the net section. Achieving a balance among the failure modes certainly provides an attractive and viable means for establishing the minimum edge distances and fastener spacing.

Plates of relatively thin cross sections, including extruded shapes fastened by one or more components, may fail by tearing of a piece of material along the periphery of the connection. Frequently, the "block shear" failure of a gusset connection plate and a single-angle member when subjected to a far-field tensile load occurs by the removal of material at and around the boundary of the bolt group. For a single-angle member, load is essentially transferred by tension along a horizontal plane defined by the edge of the member and the first mechanical fastener (bolt or rivet), while localized shearing is promoted along the line of fasteners. A similar situation exists with the gusset or connecting element. A combination of tension and shear forces develops along an area defined by the periphery of the fastener group. Another practical example that deserves consideration of block shear failure are shear connections in beams having coped flanges (Ref 4).

There is a paucity of experimental research on an understanding of the mechanisms and micromechanisms governing failure of mechanical connection(s) in pure aluminum and aluminum-base alloys. The behavior of angles fastened by a single leg was first investigated by Sharp (Ref 5). He observed the failure mode to change as a function of the number of fasteners. Marsh developed and put forth a model to estimate the capacity of bolt groups, based upon data from double-lap joints fabricated from sheet stock of aluminum alloy 6063-T6 (Ref 6). Tests were conducted on specimens having different geometry. The model used to estimate joint capacity accounted for the following variables: (a) distance around the bolt group perimeter, (b) sheet thickness, and (c) ultimate tensile strength of the base material. Excluding those joints that failed by pure shear along a single fastener line, the analytical predictions of strength generally agreed, within several percentage points, with the experimentally determined value.

The objective of this paper is to present and discuss the appropriate design criteria for response and failure of bolted connection elements in a medium strength aluminum alloy.

2. Material and Experimental Techniques

The material chosen for this study was the commercially available Al-1.0 Mg-0.60 Si alloy (Aluminum Association designation 6061) in the T6 condition. The as-received material was fully recrystallized with fairly large recrystallized grains

C.C. Menzemer, L. Fei, and **T.S. Srivatsan,** The University of Akron, Akron, OH 44325.

that were flattened and elongated in the direction of mechanical deformation (rolling) (Fig. 1). The presence of iron (0.05 wt%) as an impurity element in the alloy resulted in the precipitation of a high volume fraction of coarse iron-rich and even silicon-rich constituents during conventional casting. These particles were identified in earlier studies to be the compounds Al_7Cu_2Fe and $Al_{12}(FeMn)_3Si$ (Ref 7, 8), and they ranged in size from about 3 to 10 μm. The presence of chromium (0.20 wt%) as the grain refining element resulted in the precipitation of the dispersoids ($Al_{12}Mg_2Cr$) during ingot preheat and high temperature homogenization treatments. The chromium dispersoids aid in retaining the directional grain structure developed during mechanical deformation (rolling) of the wrought plate and also assist in preventing the excessive growth of recrystallized grains that form during subsequent heat treatments. The coarse iron-rich and silicon-rich intermetallic particles and the insoluble magnesium-rich phase (Al_2CuMg) were stratified and distributed along the longitudinal direction (rolling) of the wrought plate. The particles were also found decorating the high-angle grain boundaries (Fig. 2). Silicon and magnesium were present in balance to form the quasi-binary Al-Mg_2Si. Strengthening in this alloy arises from the presence of the magnesium silicide phase (Mg_2Si), which is the primary hardening precipitate (referred to as β′) formed during artificial aging of the alloy at temperatures ranging from 433 to 463 K. A ratio of magnesium to available silicon of 1.7 to 1 ensures that all of the solute is contained in the Mg_2Si phase (Ref 8). The excess silicon in the alloy, over and above the amount required for the formation of the ordered Mg_2Si phase, was deposited at the grain boundaries as elemental silicon.

A total of 20 gusset plates were fabricated from 6.25 mm thick plate of aluminum alloy 6061-T6. Five replicate tests were conducted for each specimen configuration. As a number of parameters (extrinsic and intrinsic) control the behavior of mechanically fastened joints in aluminum-base alloys, only few of the most influential were considered for inclusion in this study. The extrinsic parameters considered were (a) specimen

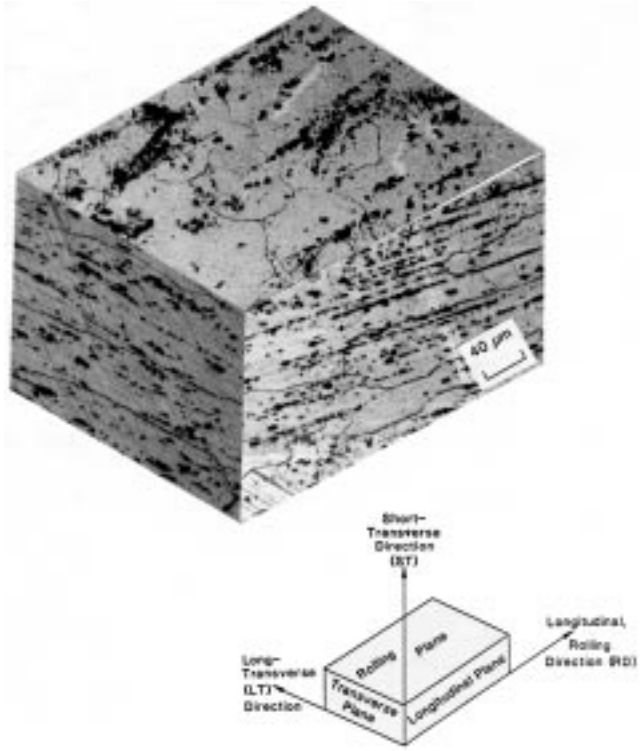

Fig. 1 Triplanar optical micrograph showing typical as-received microstructure of aluminum alloy 6061

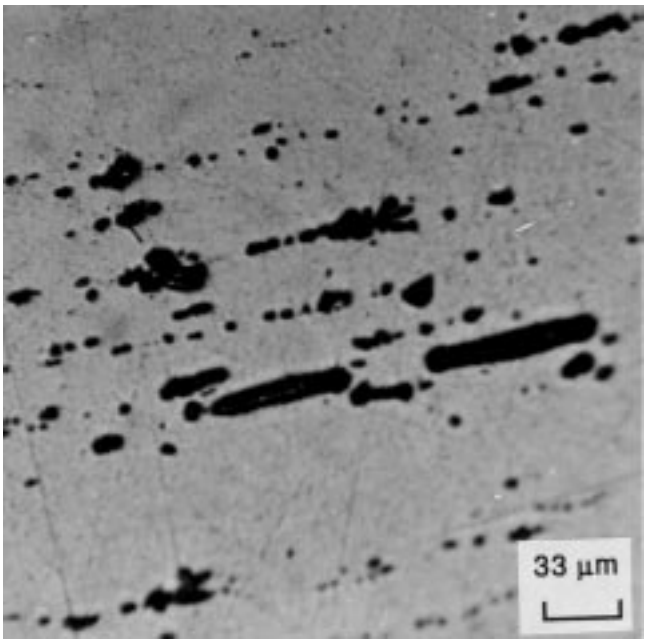

(a)

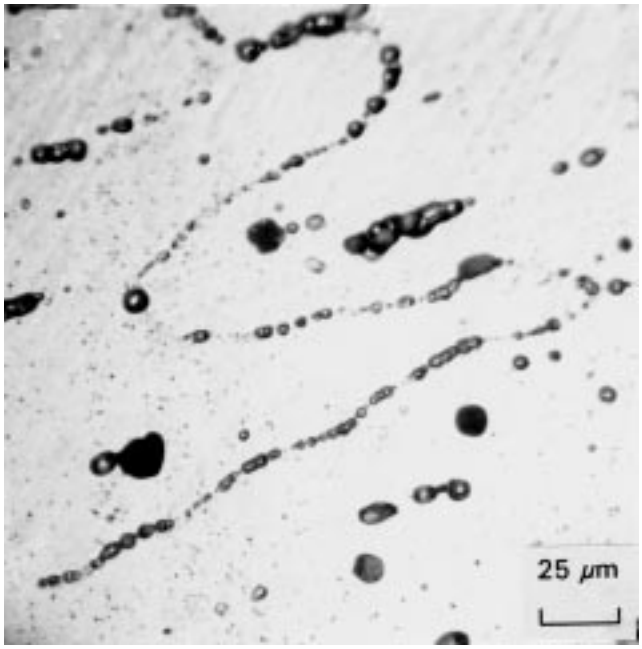

(b)

Fig. 2 Optical micrographs showing the distribution of coarse and intermediate-size particles

geometry to include variation in joint length, (b) fastener gage spacing, and (c) specimen orientation. Four different specimen configurations were examined (Fig. 3). Specimen ST1 provided for the combination of shortest gage (50 mm) and overall joint length (Fig. 3a). Gage, for this specimen configuration, refers to the distance between the lines of mechanical fasteners.

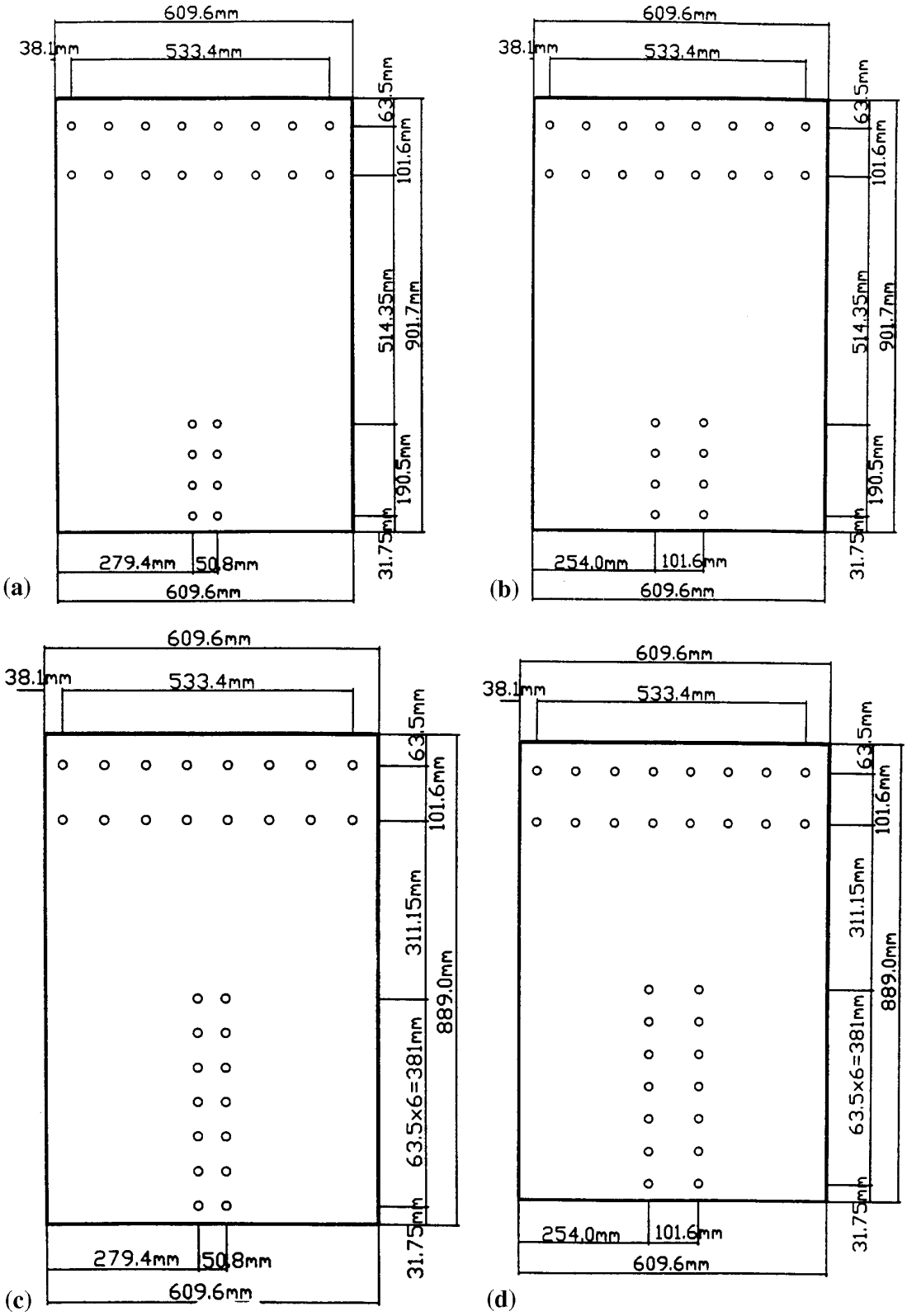

Fig. 3 Schematic showing geometry of test samples. (a) Sample ST1. (b) Sample ST2. (c) Sample ST3. (d) Sample ST4

Specimen ST2 had the same overall joint length, but twice the gage spacing (Fig. 3b). The geometry of test specimen ST3 utilized a combination of narrow gage (50 mm) with twice the overall joint length (Fig. 3c). The specimen ST4 had the largest gage spacing and joint length considered in this study.

All the mechanical tests were conducted on a 300 kip Warner-Swasey universal testing machine (UTM). Displacement was measured, at two points on the lower cross head of the test machine, by a pair of linear variable displacement transducers (LVDT). Strains were measured by mounting strain gages around the periphery of the connection. Strain gages were placed on the test specimens to lie on an outer periphery of the test fixture. Strain and displacement measurements were concurrently recorded on a Micro-Measurement data acquisition system (Ref 9). Load was read from a dynamometer at prescribed intervals and subsequently entered onto spreadsheets to provide variations of (a) load versus displacement and (b) load versus strain.

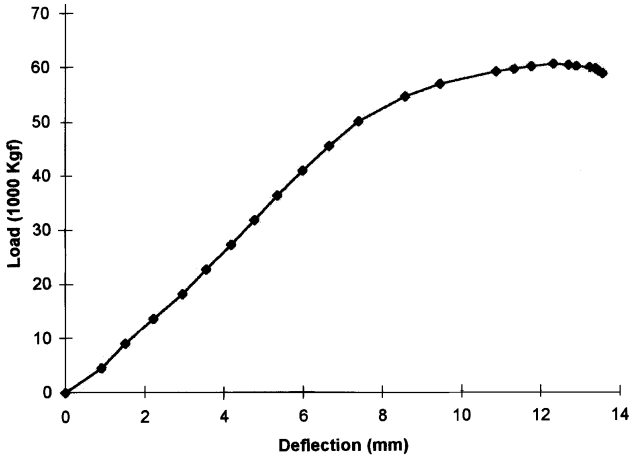

Fig. 4 Typical load-displacement behavior of a connection plate

Failure surfaces were prepared from selected samples and examined in a JEOL scanning electron microscope (SEM) in an attempt to correlate the mechanisms governing macroscopic and microscopic failure with model development. The macro-

Fig. 5 Photograph showing failure location in sample ST1-5

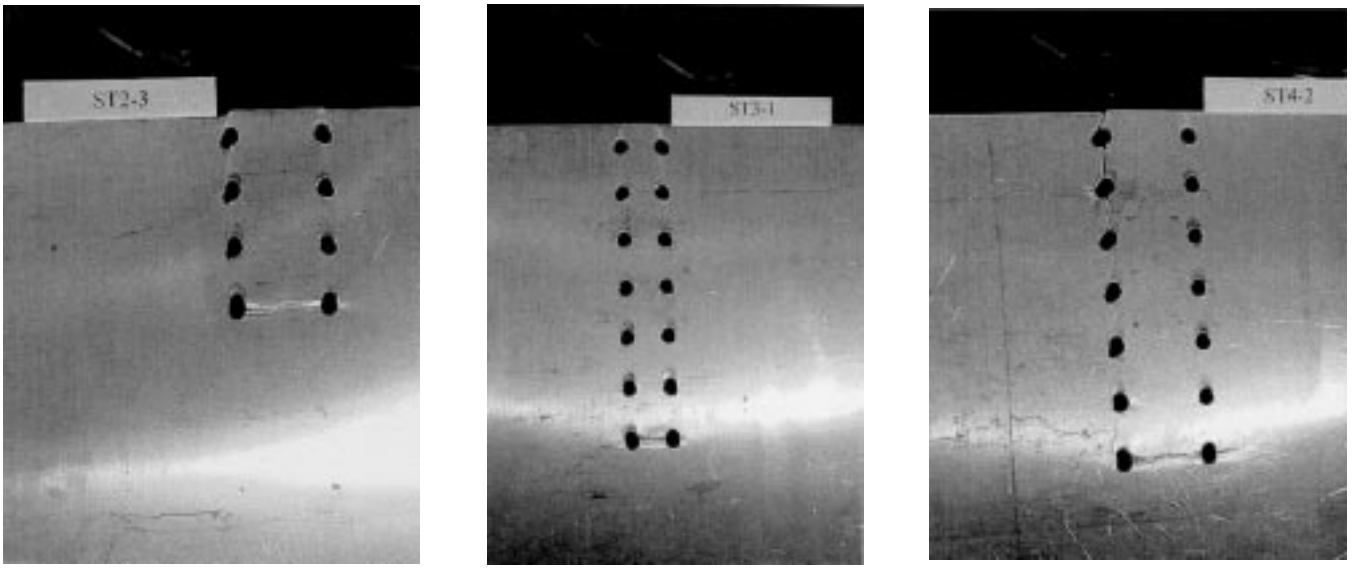

(a) **(b)** **(c)**

Fig. 6 Photographs showing failure locations in (a) sample ST2-3, (b) sample ST3-1, and (c) sample ST4-2

scopic failure mode and the intrinsic micromechanisms governing fracture were established.

3. Results and Discussion

3.1 Mechanical Deformation/Testing

Figure 4 shows a typical load versus displacement response for one gusset connection plate. The bolts were brought to a snug fit condition prior to the initiation of mechanical deformation. No effort was made to roughen the surfaces of the 6061-T6 aluminum alloy specimens, and the load was expected to be transferred predominantly by bearing. At the limit, load transfer by the bearing would be expected because many friction-type connections are proportioned at service level loads. The load versus displacement record revealed an absence of a horizontal plateau during elastic loading, considered typical of a sudden transition into bearing. Conversely, the load-displacement curves showed evidence of a progressive increase in slope during the early stages of mechanical deformation. Such behavior is indicative of the removal of slack from the load train coupled with a gradual slip into bearing. However, all of the specimens that were preloaded prior to the initiation of mechanical loading did not exhibit such behavior, and the load versus displacement record, for all practical purposes, was essentially linear in the elastic region.

Upon removal of the initial slack from the load train, the majority of test records revealed a linear load-displacement region followed by strain hardening into the plastic domain. Upon reaching the ultimate load of the gusset connection plate, the majority of test specimens exhibited a gradual drop in load carrying capability culminating in failure of one or more of the ligaments as a result of tensile overload. With continued mechanical deformation the specimens showed a sustained drop in load carrying capability until the termination of testing.

Table 1 Summary of test results

Specimen number, kgf × 10^3	Maximum load
ST1-1	50.0
ST1-2	54.0
ST1-3	52.4
ST1-4	52.6
ST1-5	52.4
ST2-1	61.0
ST2-2	62.0
ST2-3	63.4
ST2-4	62.6
ST2-5	60.0
ST3-1	90.0
ST3-2	88.5
ST3-3	88.5
ST3-4	85.0
ST3-5	88.5
ST4-1	98.0
ST4-2	98.0
ST4-3	97.0
ST4-4	95.0
ST4-5	99.0

An examination of the load-displacement response (curves) revealed the individual specimens, within each series, to exhibit similar ultimate strengths. None of the load-displacement curves exhibited a sharp yield point. However, the occurrence of yielding was gradual and quite similar to the engineering stress-engineering strain curve in a uniaxial tension test. Specimens with the shortest overall joint length (types ST1 and ST2) revealed a smaller variation in deformation as compared with the specimens belonging to types ST3 and ST4. Almost all of the test specimens belonging to the four configurations exhibited failure of the ligament as a result of tensile overload. Figure 5 shows tensile failure at the upper bolt row of sample ST1-5. Visual examination of the mechanically deformed plate revealed the occurrence of a significant decrease in cross sectional area or necking between the lines of mechanical fasteners. The concurrent occurrence of localized necking and shear left behind an orange peellike roughness on the surface of the specimens. It was also observed that the bolt holes along both the normal and shear planes were elongated. Figure 6 shows failure locations of the other sample types.

Most block shear models in current engineering practice use either a combination of tensile rupture with shear yielding or shear rupture accompanied by tensile yielding. Failure of the ligament as a result of tensile overload was observed in all of the samples tested. The occurrence of failure predominantly by shear was less significant. In several instances, the bolts were forced or pulled out through the last several holes. In most cases, there was a noticeable deformation, quantified in terms of elongation, of each hole coupled with an evidence of localized plastic deformation and yielding around the periphery of the fastener holes. The occurrence of localized plasticity and concomitant yielding left behind an orange peel roughness on the surface of the plates in the immediate vicinity of the holes.

Table 1 summarizes the results of all connection plate tests. The variation of failure load as a function of specimen type is exemplified in Fig. 7. The test results of the samples are plotted in groups of five, each representing a single specimen geometry:

- The failure load increases in traversing from left to right with the groups plotted starting with ST1, followed by ST2, ST3, and ST4.

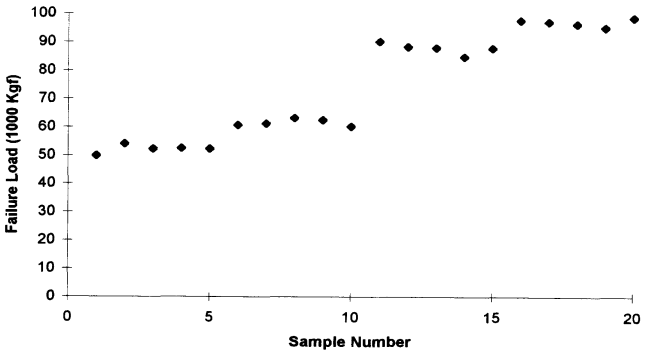

Fig. 7 Variation of failure load as a function of sample type. ST1 is represented by points 1 to 5. ST2 is represented by points 6 to 10. ST3 is represented by points 11 to 15. ST4 is represented by points 16 to 20.

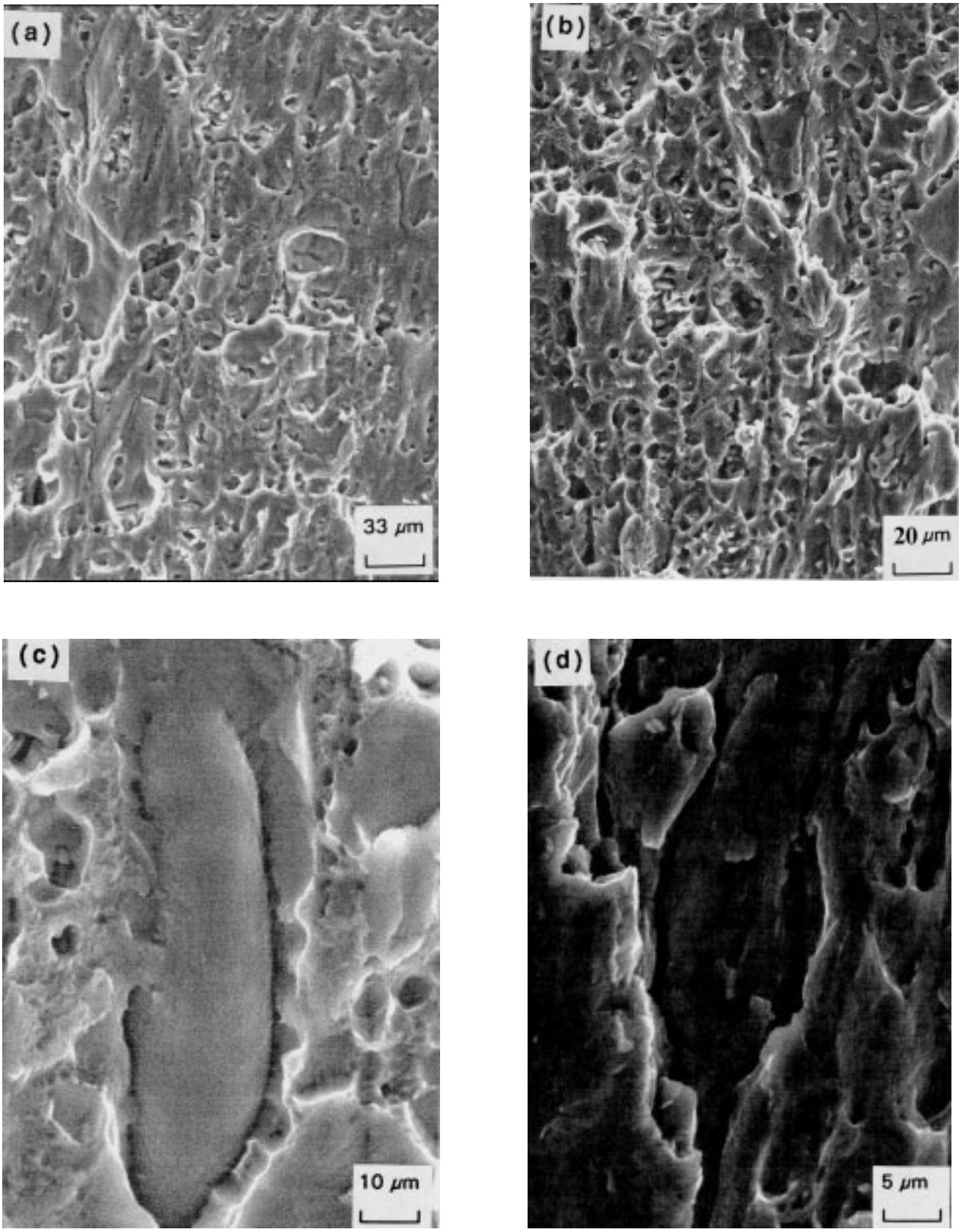

Fig. 8 Scanning electron micrographs showing fracture surface morphology of sample from ST2-2. (a) Predominantly shear failure. (b) Localized shearing, microscopic secondary cracks, and cracked particles. (c) Intergranular cracking and regions of localized microplastic deformation, reminiscent of locally ductile failure. (d) Macroscopic cracking along the high-angle grain boundary

- Specimen configuration ST2 was designed to have twice the tensile area, or twice the distance between the rows of bolts, as compared to configuration ST1. On an average, the ST2 specimen failed at a load 10.1×10^3 kgf higher than specimen type ST1.
- The ST3 specimens were chosen to have twice the overall joint length as compared to the specimens ST1 and ST2. Furthermore, the ST3 specimen possessed the same tensile area as specimen ST1. In comparison with ST1, the ST3 samples failed at loads averaging 38.9×10^3 kgf higher.
- Specimens with the ST4 geometry had the same tensile gage as specimen ST2, but with the longer connection length. However, on average, the ST4 specimens failed at loads 10.1×10^3 kgf higher than the ST3 specimens and 38.9×10^3 kgf higher than the ST2 counterpart.

3.2 Failure-Damage Analysis

Samples from the deformed and failed surfaces were carefully examined with a JEOL SEM. Figure 8 shows representative micrographs. Fracture surface features are correlated with load transfer and stress distribution within the bolt group and intrinsic microstructural effects.

Figure 8(a) shows the overall fracture surface morphology of a ST2-2 sample. This particular area of the fracture surface was removed from a region containing a macroscopic crack associated with the bottom portion of a bolt line adjacent to the edge of the specimen (Fig. 8b). The surface reveals clear evidence of elongated dimples and localized shearing. The elongation of dimples and shearing are favored by the occurrence of localized plasticity, referred to henceforth as "microplasticity," associated with intense slip band activity (i.e., formation) and resultant strain localization. A population of voids, of varying size and shape, was found distributed randomly through the fracture surface. With a increase in the applied load, the macroscopic voids progressively grew and eventually coalesced. Void coalescence was exacerbated by the formation of void sheets at the intermediate size $Al_{12}Mg_2Cr$ dispersoids and the equilibrium β matrix precipitates. The macroscopic and fine microscopic voids resulted from fracture of the second-phase intermetallic particles and the insoluble magnesium-rich phase (Al_2CuMg). The halves of the voids are the shallow dimples on the fracture surface. With continued mechanical deformation, the remaining ligament of material is inadequate to withstand the far-field load, culminating in catastrophic failure.

At an alternative location of failure, high magnification observations of the fracture surface revealed predominantly shear failure with elongated dimples and isolated pockets of localized microplastic deformation (Fig. 8c). An array of fine microscopic cracks, reminiscent of locally brittle failure mechanisms, was also found distributed through the fracture surface. The macroscopic cracks followed the intrinsically weakened high-angle grain boundaries suggesting the occurrence of brittle intergranular failure (Fig. 8d). At frequent intervals, cracked particles and decohesion at their interfaces were observed. The presence of numerous voids, of varying size and shape, and shallow dimples suggests the existence of locally ductile mechanisms. Extensive cracking along the high angle grain boundaries was associated with microscopic void formation and dimples immediately adjacent to the grain boundary regions.

3.3 Development of Failure Model

Several different free body diagrams can be visualized (Fig. 9), that isolate the connection area of a generic gusset connection plate. The primary load transfer mechanisms are (a) tension along the upper most fastener row and (b) shear along the length of both bolt lines. Differences arise as to the specific areas over which the forces act. The four most likely combinations are:

- Tension and shear acting on the gross area ($P = A_{gt} \cdot \sigma_u + A_{gv} \cdot 0.6\sigma_y$)
- Tension acting on the net area and shear acting on the gross area ($P = A_{nt} \cdot \sigma_u + A_{gv} \cdot 0.6\sigma_y$)
- Tension acting on the gross area while shear acts on the net area ($P = A_{gt} \cdot \sigma_u + A_{nv} \cdot 0.6\sigma_y$)
- Both tension and shear acting along the net area ($P = A_{nt} \cdot \sigma_u + A_{nv} \cdot 0.6\sigma_y$)

where P is the predicted failure load of the connection plate, A_{gt} is the gross tensile area, A_{nt} is the net tension area, A_{gv} is the gross shear area, A_{nv} is the net shear area, σ_U is the ultimate tensile strength, and σ_y is the tensile yield strength. The onset of yielding in monolithic metals is relatively insensitive to the hydrostatic stress component and is primarily a function of the deviator stress (Ref 10). The occurrence of yielding in pure shear is predicted when the stress reaches 0.6 times the uniaxial yield stress (Ref 11).

An evaluation of the four different free body diagrams and the resulting models is based on a previously developed methodology (Ref 12, 13). A professional factor defined as the ratio of the ultimate load, P_{ult} (determined from tests of individual samples), to the calculated model connection strength is established. This is expressed as:

$$\text{Professional Factor} = \text{Ultimate Test Load/Model Prediction}$$

An agreement between the experimental results and analytical predictions is indicated by a factor equal to or close to 1.0. Pure aluminum and aluminum alloy-based structures are typically designed on the basis of guaranteed minimum mechanical properties. Actual properties are often in excess of the guaranteed values. Hence, the model needs to be assessed not only on the basis of experimentally determined properties, but should provide conservative estimates when connection strength is calcu-

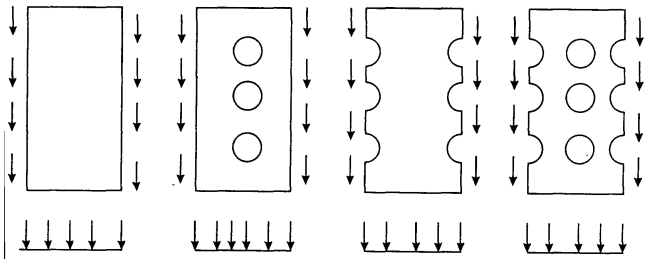

Fig. 9 Free body diagrams for the bolt group area

lated from guaranteed minimum tensile properties. A conservative result may be interpreted as a factor greater than 1.0.

Figure 10 summarizes model predictions for samples manufactured from alloy 6061-T6. The variation of professional factor with specimen number, obtained using the calculated strengths based on typical monotonic mechanical properties (Ref 14) is shown in Fig. 10(a). Specimens 1 to 5 represent geometry ST1, specimens 6 to 10 represent geometry ST2, specimens 11 to 15 represent geometry ST3, and specimens 16 to 20 represent geometry ST4. Calculated strengths from models 3 and 4 grossly underestimate the ultimate test load because the factor is significantly greater than 1.0. The connection strengths determined from models 1 and 2 tend to overestimate load carrying capacity. However, they are closer to the experimentally obtained results. Maximum deviation is of the order of 15%. A factor less than 1.0 suggests that the predicted strength is greater than experimental test results and should be considered nonconservative.

Figure 10(b) shows the results for the four models based upon experimentally determined monotonic mechanical properties. Models 3 and 4 underestimate connection plate strength, in some instances by as much as 35%. However, models 1 and 2 provide for more realistic predictions and tend to be more accurate for shorter length connections (sample numbers 1 to 10). With an increase in the connection length, the strength estimates tend to increase at a rate greater than test results. Consequently, the professional factor decreases. With an increase in the connection length the average shear stress carried by the fasteners decreases. This is particularly true for the bolts in the interior because they carry a smaller portion of the load.

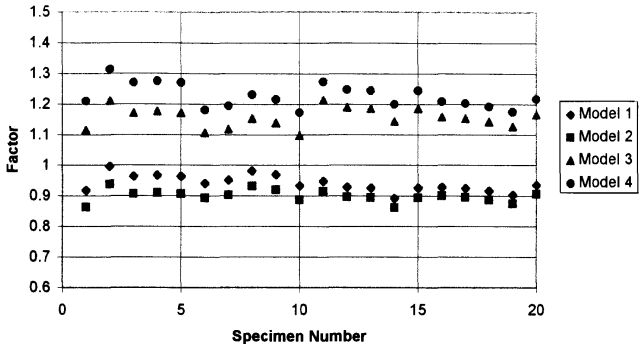

(a)

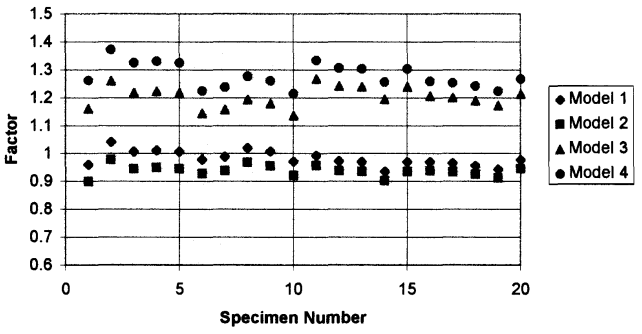

(b)

Fig. 10 Calculated professional factors of alloy 6061-T6 based upon (a) typical tensile properties and (b) experimentally determined tensile properties

4. Conclusions

Based on a study aimed at identifying the failure behavior of bolted connections in the medium strength aluminum alloy, the following salient observations were made:

- A series of tests were successfully conducted on connection plates fabricated from aluminum alloy 6061-T6.
- Block shear failure is a potential limit state for connection plates having mechanical fasteners and must be considered in all design procedures. At the limit, the shear stress is essentially uniform along the outside edges of the bolt line.
- When the tensile stresses between the upper row of bolts reach a particular value, the failure or rupture of the ligament between the fastener holes is promoted.
- Fractography of the fracture surfaces revealed the damage accumulation mechanisms to be consistent with the assumptions used in the development of a predictive model.

Acknowledgment

The authors extend their sincere thanks to The Aluminum Association (Washington, D.C.) for financial support of this research and to The University of Akron (Akron, OH) for providing a tuition scholarship to Ms. Lei Fei.

References

1. American Association of State Highway and Transportation Officials, AAASHTO LRFD Bridge Design Specifications, Section 7—Aluminum Structures, Washington, D.C., 1994
2. *The Aluminum Design Manual,* The Aluminum Association, 1994
3. J.W. Fisher and J.H. Struik, *A Guide to Design Criteria for Bolted and Riveted Joints,* John Wiley & Sons, Inc., 1974
4. P.C. Birkemoe and M.J. Gilmor, Behavior of Bearing Critical Double-Angle Beam Connections, *AISC Eng. J.*, American Institute of Steel Construction, Vol 4, 1978
5. M.L. Sharp, *A Behavior and Design of Aluminum Structures,* McGraw-Hill, 1993
6. C. Marsh, Tear-Out Failure of Bolt Groups, American Society of Civil Engineers, *ASCE Structural J.*, No. ST10, Oct 1979
7. E.A. Starke, Jr., *Mater. Sci. Eng.*, Vol 29, 1977, p 99-115
8. E.A. Starke, Jr., Aluminum Alloys: Contemporary Research and Applications, *Treatise in Materials Science and Technology,* Vol 31, A.K. Vasudevan and R.D. Doherty, Ed., Academic Press, 1989, p 35
9. "Measurements Group: A System 5000 Model 5100 Scanner—Instruction Manual," Instruments Division, Raleigh, NC, 1995
10. W.F. Chen and D.J. Han, *Plasticity for Structural Engineers,* Springer-Verlag, 1988
11. R.W. Hertzberg, *Deformation and Fracture Mechanics of Engineering Materials,* 2nd ed., John Wiley & Sons, 1983
12. S. Haradash and R. Bjorhoude, New Design Criteria for Gusset Plates in Tension, *AISC Eng. J.*, American Institute for Steel Construction, Vol 2, 1985
13. T.V. Galambos, Load and Resistance Factor Design, *AISC Eng. J.*, American Institute for Steel Construction, Vol 3, 1981
14. *Aluminum Standards and Data, The Aluminum Association,* 1988